NANO LETTERS
Cite This: Nano Lett. 2018, 18, 3926−3933
Letter
pubs.acs.org/NanoLett

Three-Dimensional, Solid-State Mixed Electron−Ion Conductive Framework for Lithium Metal Anode

Shaomao Xu,[†,‡] Dennis W. McOwen,[†,‡] Chengwei Wang,[†,‡] Lei Zhang,[†,‡] Wei Luo,[‡] Chaoji Chen,[‡] Yiju Li,[‡] Yunhui Gong,[†,‡] Jiaqi Dai,[†,‡] Yudi Kuang,[‡] Chunpeng Yang,[†,‡] Tanner R. Hamann,[†,‡] Eric D. Wachsman,*[,†,‡] and Liangbing Hu*[,†,‡]

[†]Maryland Energy Innovation Institute, College Park, Maryland 20742, United States
[‡]Department of Materials Science and Engineering, University of Maryland, College Park, Maryland 20742, United States

Supporting Information

ABSTRACT: Solid-state electrolytes (SSEs) have been widely considered as enabling materials for the practical application of lithium metal anodes. However, many problems inhibit the widespread application of solid state batteries, including the growth of lithium dendrites, high interfacial resistance, and the inability to operate at high current density. In this study, we report a three-dimensional (3D) mixed electron/ion conducting framework (3D-MCF) based on a porous-dense-porous trilayer garnet electrolyte structure created via tape casting to facilitate the use of a 3D solid state lithium metal anode. The 3D-MCF was achieved by a conformal coating of carbon nanotubes (CNTs) on the porous garnet structure, creating a composite mixed electron/ion conductor that acts as a 3D host for the lithium metal. The lithium metal was introduced into the 3D-MCF via slow electrochemical deposition, forming a 3D lithium metal anode. The slow lithiation leads to improved contact between the lithium metal anode and garnet electrolyte, resulting in a low resistance of 25 Ω cm^2. Additionally, due to the continuous CNT coating and its seamless contact with the garnet we observed highly uniform lithium deposition behavior in the porous garnet structure. With the same local current density, the high surface area of the porous garnet framework leads to a higher overall areal current density for stable lithium deposition. An elevated current density of 1 mA/cm^2 based on the geometric area of the cell was demonstrated for continuous lithium cycling in symmetric lithium cells. For battery operation of the trilayer structure, the lithium can be cycled between the 3D-MCF on one side and the cathode infused into the porous structure on the opposite side. The 3D-MCF created by the porous garnet structure and conformal CNT coating provides a promising direction toward new designs in solid-state lithium metal batteries.

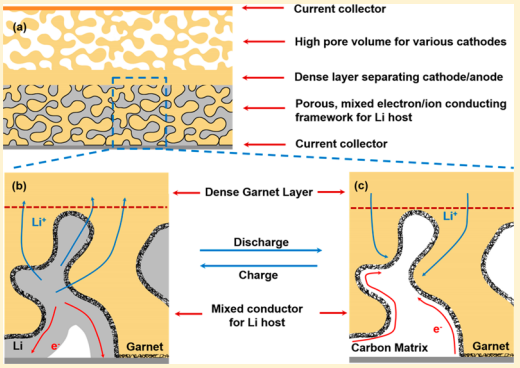

KEYWORDS: *3D lithium, solid state battery, mixed electron/ion conductor, garnet electrolyte, lithium metal anode, high current lithium cycling*

Downloaded via YALE UNIV on January 26, 2026 at 04:30:21 (UTC).
See https://pubs.acs.org/sharingguidelines for options on how to legitimately share published articles.

Society's demand for energy storage devices has dramatically increased during the past few decades due to the ever-increasing development of portable electronic devices, electric vehicles, and grid level energy storage. The search for high-energy density battery systems to meet today's energy storage needs has become a high priority area of research.[1−6] Lithium metal is the most promising anode for next-generation batteries due to its lowest weight among all metals (0.53 g/cm^3), the most negative electrochemical potential (−3.04 V vs SHE), and the highest specific capacity (3860 mAh/g).[7−9] With conventional organic electrolytes, the largest obstacles prohibiting the application of lithium metal anodes are the infinite volume change and dendrite growth on the lithium metal surface while the cell is charging.[7,10−12] Specifically, the volume change of lithium metal during battery cycling leads to repeated breaking and reformation of the solid electrolyte interface (SEI), which consumes a considerable amount of electrolyte, resulting in low Coulombic efficiency, and can increase cell resistance. Moreover, upon long-term battery operation the deposition of lithium metal is not uniform. Instead, a dendritic structure at the surface of the anode forms, which eventually bridges the anode and the cathode, leading to internal short circuits. Significant effort has been devoted to resolving the safety issues caused by lithium dendrite growth, including the employment of electrolyte additives,[12] engineering of separators,[13−17] and theoretical studies of lithium deposition.[18,19] One promising approach is to confine the lithium within a 3D anode network,[20−27] which effectively contains the lithium stripping/plating inside the anode framework so the dendrites

Received: March 30, 2018
Revised: May 16, 2018
Published: May 22, 2018

© 2018 American Chemical Society

DOI: 10.1021/acs.nanolett.8b01295
Nano Lett. 2018, 18, 3926−3933

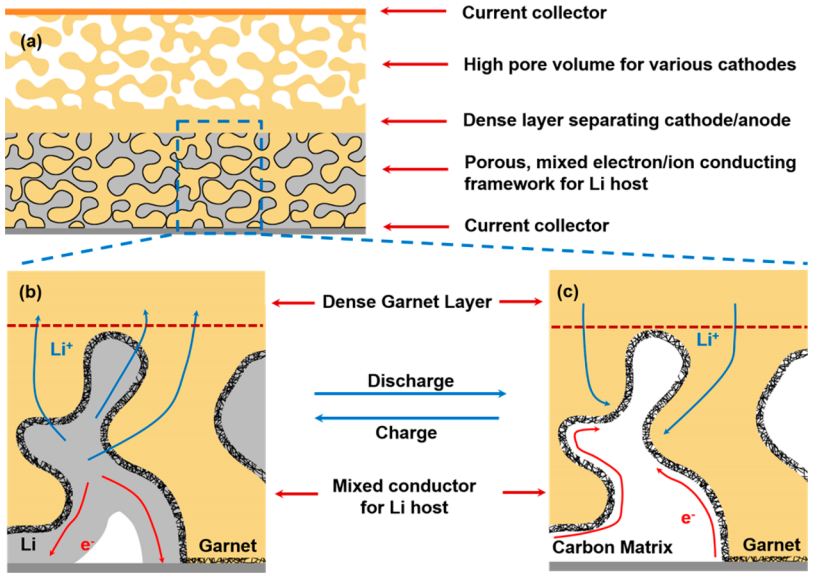

Figure 1. Schematic demonstrating the working principle of the 3D lithium metal anode based on a 3D-MCF. (a) Structure of the porous−dense−porous trilayer garnet framework with a mixed electron/ion conductor incorporated on the anode side. (b) Working mechanism on the anode side during (b) discharge and (c) charge.

cannot form toward the separator, leading to massively improved long-term stable cycling.[21,22]

One solution to the lithium metal problem is the employment of a solid-state electrolyte (SSE), which can physically block the growth of lithium dendrites and prevent short circuits.[28−30] Many types of SSEs have been extensively studied during the past few years, including perovskite type electrolytes,[31,32] NASICON type electrolytes,[33,34] garnet-based electrolytes,[35−38] and sulfide-based electrolytes.[39,40] Among these materials, cubic phase garnet type electrolytes have shown excellent performance due to their high ionic conductivity and electrochemical stability to both lithium metal and a variety of cathodes. Massive progress has been achieved for the application of SSEs, including increasing the ionic conductivity of the electrolyte,[37,38] reducing the anode interfacial resistance,[41−43] and improving contact between electrolyte and cathode.[44−46] However, recent studies show that lithium dendrites can still grow while using SSEs when the battery is operated under a high current density,[2,47] leading to the possible penetration of lithium through the SSE and formation of a short circuit between the anode and cathode. Researchers have hypothesized that lithium can grow along grain boundaries or open pores of the SSE[2] and surface-induced dendrite penetration,[47] but the mechanism of lithium dendrite propagation through SSEs remains unclear. There is a lack of study on 3D Li hosts with SSEs due to the poor contact between the electrolyte and the electrode. A 3D solid state lithium metal anode can enable high current density operation by multiplying the anode−garnet interfacial area. This can result in much improved performance to enable a range of battery chemistries. Therefore, an SSE coupled with a 3D anode framework could be a promising route for the practical application of Li metal as battery anode.

We have previously designed a porous−dense−porous trilayer garnet structure, where a 30 μm thick dense garnet layer is sandwiched between two porous garnet frameworks each with a thickness of 60 μm.[48] Here for the first time, we designed a 3D mixed electron/ion conducting framework (3D-MCF) using the garnet electrolyte as the lithium host, thus enabling a solid-state lithium metal anode. The concept of the trilayer with a 3D-MCF design is shown in Figure 1. Carbon nanotubes (CNTs) are uniformly coated into the pores on one side of the trilayer structure, introducing electronic conductivity on the surface of garnet electrolyte within the framework. With the ionic conductivity provided by the SSE, lithium ions flow in the garnet electrolyte while electrons flow along the CNTs at the surface, thus forming a mixed electron/ion conducting framework. With slow electrochemical deposition, lithium metal can be uniformly infused into the 3D-MCF to form the 3D lithium metal anode in the garnet framework, which ensures seamless contact between the electrolyte and the lithium anode. During battery discharging, the lithium on the anode side releases an electron and forms a lithium ion. The electron transfers along the CNT layer and the lithium metal to the current collector, while the lithium ion transfers through the garnet framework to reach the cathode side. During the charging process of the battery, the cathode expels a lithium ion, which transfers through the dense garnet layer and receives an electron to form lithium metal on the anode side. The utilization of the 3D-MCF brings multiple advantages to the solid-state lithium metal battery design. First, due to the 3D lithium host, lithium growth is confined within the porous structure. Therefore, unlike conventional lithium metal batteries, lithium dendrites only grow within the pores and do not penetrate the dense center layer to bridge the anode and cathode, preventing short circuit of the battery. Moreover, with the improved contact due to the mixed electron/ion conductivity, and the 40 times higher specific surface area from the porous architecture of the garnet framework,[48] stable lithium cycling is possible under much higher areal current density and has been demonstrated in a symmetric lithium cell at 1 mA/cm^2 based on the geometric area of the cell for 200 h. Additionally, with the high porosity of the porous garnet structure, the trilayer garnet with 3D-MCF can enable a range of cathode chemistries with a low impedance and potentially high current density. As a proof of concept, we introduce a lithium polysulfide battery based on the trilayer structure.[49] The solid nature of the ceramic electrolyte prevents the lithium

DOI: 10.1021/acs.nanolett.8b01295
Nano Lett. 2018, 18, 3926−3933

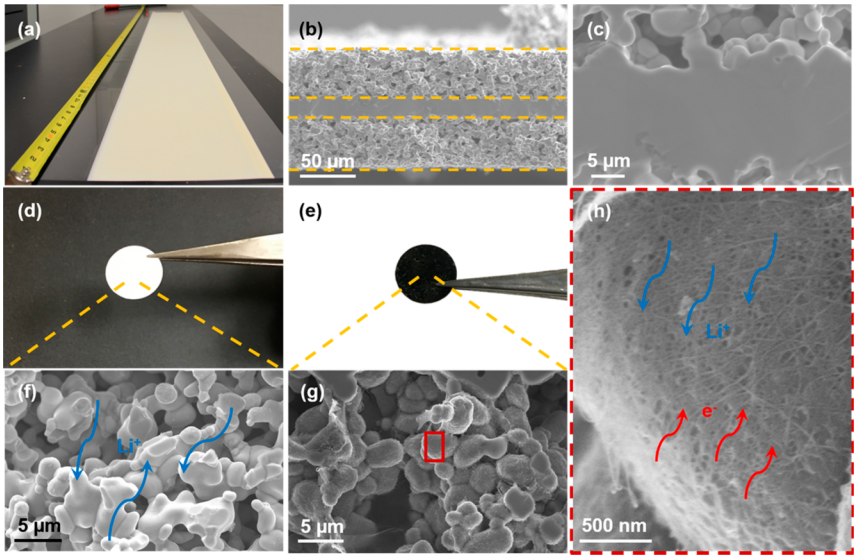

Figure 2. Characterization of the trilayer garnet SSE with anode 3D-MCF. (a) Photo of a LLZ garnet tape. (b) Cross-sectional SEM image of the garnet electrolyte showing the trilayer structure. The thickness of the dense layer and the porous layers are 30 and 60 μm, respectively. (c) Zoomed-in SEM image of the dense layer and the connection between the dense and porous layers. (d) Photo image of the pristine trilayer garnet pellet. (e) Photo image of the trilayer garnet pellet after CNT infiltration by solution. (f) SEM images of the trilayer garnet pellet before CNT infiltration showing smooth surface of the garnet framework. (g) SEM image of the trilayer garnet pellet after CNT infiltration showing rough surface due to the CNT coating. (h) High-magnification SEM images of the trilayer garnet pellet after CNT infiltration showing the interconnected CNT network on the garnet surface.

polysulfide from reaching the anode side, thus eliminating any polysulfide shuttle effect. The demonstrated lithium polysulfide battery was stably cycled for over 50 cycles under a high current density of 1 mA/cm^2 under a controlled capacity of 3 mAh/cm^2. The trilayer SSE structure, all-solid-state Li metal anode, and the mixed electron/ion conducting framework depict a massive improvement to our previous work.[50] This unique battery structure introduces a new direction for the design of high performance lithium metal battery for practical applications.

Characterization of the trilayer garnet based SSE with 3D-MCF anode is shown in Figure 2. The trilayer garnet was synthesized via tape casting, which is highly scalable (Figure 2a). The garnet tape was cut into pieces and sintered into coin cell size ceramic plates, which see a shrinkage rate of 37% (Figure S1). The SEM image of the trilayer electrolyte indicates a dense layer of 30 μm with 60 μm thick porous layers on either side (Figure 2b). Focusing on the dense layer, there are no pinholes that bridge the anode side and the cathode side, suppressing dendritic growth directly through the cell (Figure 2c). On the borderline between the dense layer and the porous layer, the garnet grains of the porous layer are strongly bound to the dense layer with no gaps in between. The seamless connection between these layers ensures that the lithium ions can be successfully transported between the cathode and anode without introducing extra impedance. From the top view of the porous layer, 1−10 μm sized pores can be observed (Figure S2), leading to a high energy density battery system. From the backscattering image of the porous layer, the porosity is determined to be 66% (Figure S3). Although the structure of the SSE is sophisticated, the phase purity and bulk properties of the garnet electrolyte are still maintained. The X-ray diffraction (XRD, Figure S4) on the synthesized trilayer electrolyte matches perfectly with cubic phase LLZ garnet, ensuring remarkable ionic conductivity of the bulk electrolyte. XPS data also confirms the chemistry of the garnet. The survey scan (Figure S5) indicates the existence of lanthanum (La), zirconium (Zr), and niobium (Nb) in the sintered trilayer pellets. The detailed scans (Figure S6) show that the characteristic peaks of La, Zr, and Nb matches cubic phase garnet electrolyte.

A 3D-MCF was developed by repeatedly casting CNT ink into the pores on one side of the porous-dense-porous trilayer structure until the garnet on that side was totally covered by CNTs (Figure 2d,e). Therefore, with the ion conductivity provided by the garnet electrolyte and electron conductivity introduced by the conformal CNT coating the mixed electron/ion conductivity was achieved. The morphology of the 3D framework after the infiltration of lithium and CNT was studied by SEM. Before CNT coating, the porous layer is composed of interconnected garnet grains with a smooth surface, which form micrometer-sized pores (Figure 2f). After CNT coating, the interconnected garnet structure does not change but the surface of the garnet grains became much rougher (Figure 2g). With the micrometer-sized pores, the CNT ink can freely diffuse in the porous layer, resulting in a uniform coating of CNT on the garnet surface. The elemental mapping (Figure S7) shows identical distribution of carbon and lanthanum, indicating the uniformity of the CNT coating. The magnified SEM image on a garnet grain shows that the garnet is densely and uniformly covered with CNTs, which form a continuous network of pathways for electron transport (Figure 2h). The trilayer garnet structure and the 3D-MCF together build the backbone for a 3D solid-state battery system.

The empty pores on the opposite side of the trilayer garnet from the 3D-MCF were filled with lithium to provide the lithium source for electrochemical deposition to the 3D-MCF. Lithium was infiltrated into the empty porous garnet after first using a zinc oxide (ZnO) coating to change the surface energy between the lithium metal and the garnet electrolyte.[51] A small amount of Li metal remains on top of the porous garnet framework, which only acts as current collector and does not

DOI: 10.1021/acs.nanolett.8b01295
Nano Lett. 2018, 18, 3926−3933

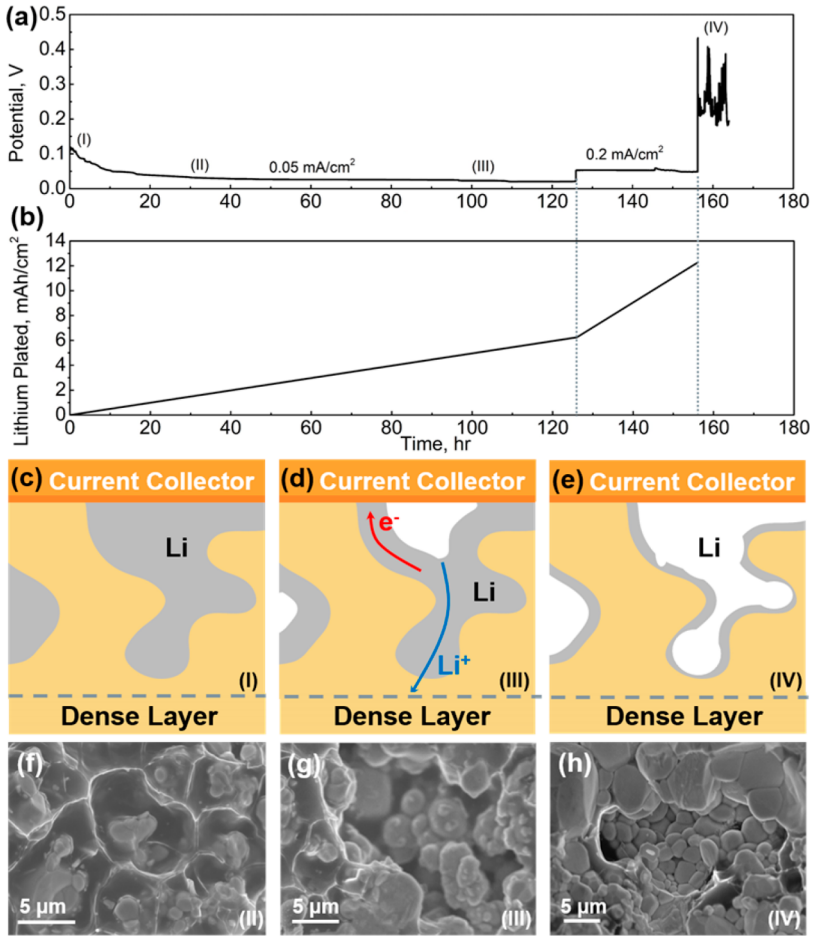

Figure 3. Lithium depletion in porous garnet framework. (a) The voltage profile of the electrochemical deposition of lithium into the 3D-MCF. (b) The accumulation of lithium plated into the 3D-MCF. (c–e) Schematics showing the process of lithium stripping from the porous garnet framework at stages I, III, IV. (f–h) SEM image of the lithium stripping side before stripping of Li (f, I), after 4 mAh/cm^2 stripping (g, III), and after depletion of Li (h, IV).

participate in the following electrochemical reaction. Lithium was then continuously plated across the cell to the CNT-coated porous garnet framework to form a lithium metal anode hosted in the 3D-MCF. During this process, lithium was continually stripped from the ZnO-coated lithium side (stripping side) and plated to the CNT side (plating side) in the all-solid-state system (Figure 3a). Here, in order to be consistent with the conventional lithium depletion test, the absolute value of the potential is shown in the figure. The original voltage profile which reflects the behavior of plating Li to CNT is shown in Figure S8. Several identical cells were tested and disassembled at different stages to study the morphology in the porous structure with the progression of lithium plating. Initially, lithium metal completely filled the pores of the stripping side while the garnet grains on the plating side are only coated with CNTs. Therefore, the voltage during the first stage of lithium plating was high but consistent with Li–C potential (0.1–0.2 V). The plating was started with a low current density (0.05 mA/cm^2) and increased by four times (0.20 mA/cm^2) once the overpotential was reduced to 20 mV, indicating there was enough plated lithium to ensure good contact on the plating side. The reaction $Li \rightarrow Li^+ + e^-$ happens on the stripping side of the cell, where the lithium ions transport within the garnet framework through the dense layer to the CNT side. After meeting the electrons traveling along the CNT, the lithium ions lithiate the CNT first. After 40 h of stripping, the CNT on the lithium plating side was lithiated and the overpotential stabilized at a lower potential of 30 mV. Lithium metal was then gradually deposited in the pores on the CNT side, so eventually the lithium stripping side was exhausted and the voltage profile became unstable (Figure 3a). With a thicker porous layer of 90 μm, 12 mAh/cm^2 of lithium was plated into the CNT side of the trilayer, forming a 3D lithium metal framework in a mixed electron/ion conductor (Figure 3b).

The morphology change of the lithium stripping side during the electrochemical test is shown in the schematics in Figure 3c–e and studied via SEM under different stages of lithium plating (Figure 3f–h). Initially before the stripping (Stage I), the pores are almost completely filled with Li metal (Figure 3c,f). Because lithium metal is both an electron conductor and Li ion conductor, all of the lithium metal in the porous layer is accessible. Therefore, Li metal both in contact with garnet and at the center of the pores can be stripped during the electrochemical test. With the continuous stripping of Li, more space is freed in the porous structure. After stripping 4 mAh/cm^2 of Li (Stage III), the vacant space in the porous structure is clearly visible (Figure 3d,g). The electrochemical test was terminated when almost all of the lithium was stripped from the anode side and the voltage profile became unstable (Stage IV). At this stage, the lithium side is almost depleted and bare garnet grains can be observed (Figure 3e,h).

DOI: 10.1021/acs.nanolett.8b01295
Nano Lett. 2018, 18, 3926–3933

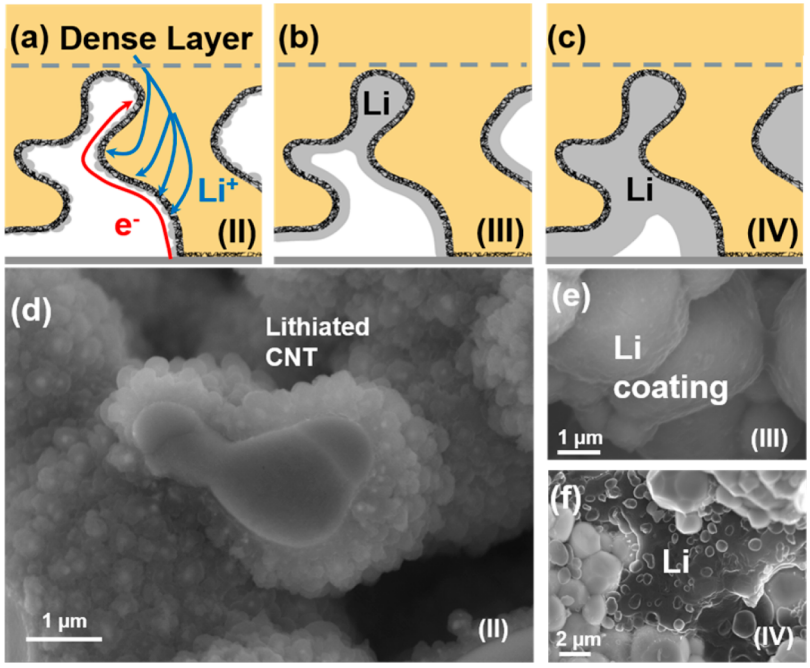

Figure 4. Growth of lithium in 3D-MCF. (a–c) Schematics showing the process of lithium plating into the porous garnet framework. (d–f) SEM image of lithium plating side of the trilayer after 1.5 mAh/cm^2 of plated Li (d), after 4 mAh/cm^2 of plated Li (e), and after the depletion of stripping side (f).

The morphology on the lithium plating side (the 3D-MCF) during the test is shown in Figure 4. Initially, there is no lithium metal (Stage I) and only garnet coated with CNTs can be observed (Figure S9). Shortly after the lithiation of the CNTs begins (1.5 mAh/cm^2, Stage II), bubble-like structures emerge evenly on top of the CNT layer (Figure 4a, d). Such unique morphology indicates the uniform lithium growth in the 3D-MCF. After the full lithiation of the CNTs, lithium metal starts to accumulate on the CNT layer with the continuous lithium plating. When 4 mAh/cm^2 of lithium is plated (Stage III), all the garnet grains on the CNT side are covered by a thick layer of lithium metal (Figure 4b, e). With the stripping side depleted (Stage IV), lithium nearly fills the pores of the CNT side (Figure 4c, f). The lithium plating study demonstrates that the trilayer garnet SSE is capable of transferring lithium from the anode to the cathode and can be used as a platform for lithium metal batteries. Moreover, the plated lithium in the 3D-MCF forms a unique 3D lithium metal anode and can enable various cathode reactions for solid state batteries.

The 3D lithium anode based on the garnet framework was also evaluated via repeated lithium metal stripping and plating. Before cycling, the CNTs were slowly prelithiated, improving the contact between the lithium and garnet leading to a low initial resistance of 25 Ω cm^2, as measured by EIS. After over 180 h of lithium cycling under a high current density of 1 mA/cm^2 based on the geometric area, the voltage profile remains stable and no short circuit was observed (Figure 5a). The voltage profiles of individual stripping/plating cycles contain flat plateaus at 20 mV (Figure 5b). Considering the 1 mA/cm^2 current density, the total resistance is calculated to be 20 Ω cm^2, which is consistent with the EIS measurement (Figure 5c). With continued lithium cycling, the contact was further improved reducing the total resistance from initially 25 Ω cm^2 to 20 Ω cm^2. Even higher current density can be achieved with the 3D-MCF architecture. Stable Li cycling with a current density of 3 mA/cm^2 and a controlled capacity of 3 mAh/cm^2 was achieved with the 3D-MCF cell (Figure S10). After over 140 h of Li stripping/plating, no overpotential change was observed, indicating the capability of high current density operation enabled by 3D-MCF. The achieved high current density can be attributed to the 3D contact area between lithium metal and garnet electrolyte. Because of the porous structure, the contact area between lithium and garnet electrolyte is 40 times higher compared to a dense pellet.[44] Therefore, with the same local current density the macroscopic areal current density can be 40 times higher compared to a conventional dense pellet. With such long lithium cycling and low resistance, the lithium metal hosted in a 3D-MCF shows significant potential for solid-state batteries.

The lithium metal in 3D-MCF with a unique porous–dense–porous trilayer structure also enables a range of cathode chemistries. We used a lithium polysulfide battery as a model system to demonstrate the application of the 3D lithium metal framework. In such a system, the dense garnet layer blocks the transport of lithium polysulfide, thus eliminating the polysulfide shuttle effect. During the discharging process, lithium metal gives away an electron and forms a lithium ion on the anode side. The lithium ion diffuses through the dense garnet layer and reacts with high order lithium polysulfide (Li_2S_8) on the cathode to form low order lithium polysulfide (Li_2S_4). During the charging process, the reverse occurs: the low order lithium polysulfide on the cathode side releases a lithium ion and forms high order lithium polysulfide. The lithium ion then diffuses through the dense layer and receives an electron to form lithium metal and deposit in the 3D-MCF. Similar to the lithium cycling in Figure 4, the high surface area of the anode framework enables a high current density operation of 1 mA/cm^2 for the full battery. The fabricated lithium polysulfide battery shows stable charge/discharge profile for over 50 cycles (Figure 5d). The charge/discharge plateaus are 2.40 and 2.17 V, respectively, which are typical charge/discharge voltages of the conversion reaction between low and high order lithium

DOI: 10.1021/acs.nanolett.8b01295
Nano Lett. 2018, 18, 3926–3933

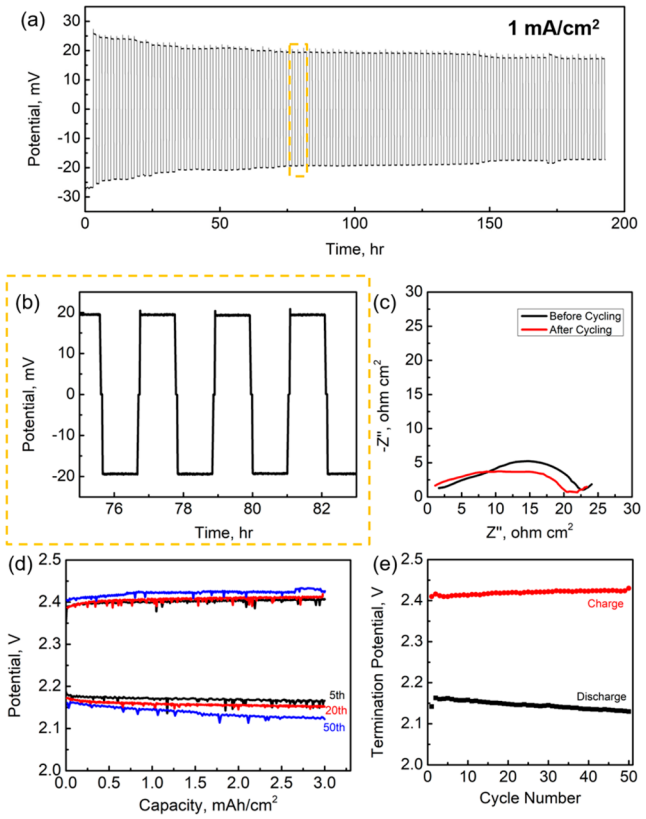

Figure 5. Electrochemical performance of the 3D lithium metal anode based on trilayer garnet framework. (a) Voltage profile of the lithium cycling in the trilayer garnet structure with 3D-MCF. (b) Zoom-in view of the voltage plateau of stripping and plating of lithium metal. (c) EIS measurement of the trilayer cell with 3D-MCF before and after lithium cycling. The decrease in resistance is due to the lithiation of CNT. (d) Charge/discharge profile of the lithium polysulfide battery under a current density of 1 mA/cm^2 with a capacity cutoff of 3 mAh/cm^2. (e) The change of discharge and charge potential with cycle number showing overpotential change less than 50 mV after 50 cycles.

polysulfide. The trilayer architecture eliminates the shuttle effect and unstable lithium deposition, leading to negligible performance decay even after 50 cycles. The change in the overpotential is less than 50 mV after 50 cycles (Figure 5e). With the scalability of the trilayer framework, the long cycle life with low overpotential makes the lithium polysulfide battery with 3D lithium metal anode in a garnet framework an excellent platform for energy storage systems.

Experimental Section. *Fabrication of Garnet Trilayer.* Isopropanol (21 wt %), toluene (21 wt %), fish oil (0.5 wt %), and the prepared LLZ (30 wt %) were weighed into a bottle with YSZ grinding media and milled for 24 h. Subsequently, benzyl butyl phthalate (BBP, 6.5 wt %) and polyvinyl butyral (PVB, 5.0 wt %) were added and milled for another 24 h. After the second day of milling was complete, 10 μm cross-linked PMMA spheres (16 wt %) were added as porogens. This slurry was milled for 1 h then degassed under 25 inHg vacuum for 3 h. Similar mixtures were made without PMMA for the dense layer tape. Slurries were cast at 10 cm/min through a doctor blade onto a mylar sheet. The tapes were then laminated together by pressing at 170 psi and 60 °C for 15 min to form multilayer structures. Circles (1.6 cm) and squares (1.3 cm, Figure S1) were cut from the laminated tapes and sintered at 1050 °C for 1 h.

Fabrication of 3D-MCF. The 3D-MCF was developed by infiltrating CNT ink (1 mg/mL, CarbonSolutions) repeatedly into the porous layer of the trilayer garnet until the surface of the trilayer was completely black. Lithium metal was infiltrated into the other side of the porous layer with ZnO surface treatment. The CNT was then lithiated by slow electrochemical plating of lithium. Eventually all the CNT was lithiated and the pores on the plating side was filled by lithium, forming the 3D-MCF.

Fabrication of Lithium Polysulfide Battery. The 3D-MCF was directly employed as the anode of the lithium polysulfide battery. A stainless steel current collector was attached to the lithium metal side and tightly sealed with wax to prevent contact with the lithium polysulfide solution. On the cathode side, CNT was infiltrated in the porous structure to provide electronic conductivity. The assembled cell was immersed in a lithium polysulfide catholyte (0.5 M) and connected to the battery tester.

Electrochemical Test of Lithium Polysulfide Cell. The electrochemical test was performed with a BioLogic battery testing system. A capacity-controlled scheme was employed for the test. The cell was cycled under a current density of 1 mA/cm^2 and a controlled capacity of 3 mAh/cm^2, that is, a single discharge or charge step is 3 h (6 h per cycle).

Material Characterization. SEM images were captured with a Hitachi SU-70 FEG SEM. The XRD patterns were obtained with a Bruker D8 Advance system. Raman spectrum were obtained with an Yvon Jobin LabRam ARAMIS. XPS spectra were obtained using a high sensitivity Kratos AXIS 165 spectrometer.

For the first time, lithium hosted in a 3D solid state mixed electron/ion conductive framework has been demonstrated with a porous-dense-porous garnet structure. The porous garnet framework synthesized via the tape casting method provides ionic conductivity while conformal CNT coating on the surface provides electronic conductivity, thus forming a mixed electron/ion conductor as a 3D host for lithium metal. The 3D lithium metal anode is formed by slow prelithiation of the CNTs in the porous garnet media. With uniform coating on the garnet surface, unique lithium deposition behavior was observed. Lithium grows evenly on the surface of the 3D-MCF, eventually filling the pores completely. The slow prelithiation leads to good contact between the lithium and the garnet electrolyte, thus improving the interface between the anode and electrolyte, resulting in a low total resistance of 20 Ω cm^2. Additionally, the trilayer architecture enables stable lithium cycling under higher current density due to the high surface area introduced by the porous garnet structure. During repeated stripping/plating test, the cell was operated under a high current density of 1 mA/cm^2 for over 180 h. Moreover, a lithium polysulfide battery was also demonstrated based on the trilayer architecture as a proof of concept to show the feasibility of using the 3D-MCF as a lithium host in solid-state lithium metal anode. The battery was stably cycled for over 50 cycles at 1 mA/cm^2 without performance decay. The 3D lithium framework based on a trilayer garnet structure is promising for the development of a high performance solid state battery.

■ ASSOCIATED CONTENT

Supporting Information

The Supporting Information is available free of charge on the ACS Publications website at DOI: 10.1021/acs.nanolett.8b01295.

DOI: 10.1021/acs.nanolett.8b01295
Nano Lett. 2018, 18, 3926−3933

Photo image showing the sintering process, XRD and XPS characterization of trilayer garnet, additional SEM images of 3D-MCF, and high current density Li cycling performance (PDF)

AUTHOR INFORMATION

Corresponding Authors

*E-mail: binghu@umd.edu.
*E-mail: ewach@umd.edu.

ORCID

Chaoji Chen: 0000-0001-9553-554X
Chunpeng Yang: 0000-0001-7075-3356
Eric D. Wachsman: 0000-0002-0667-1927
Liangbing Hu: 0000-0002-9456-9315

Author Contributions

S.X. and D.W.M. contributed equally to this work. S.X., E.D.W., and L.H. designed the project. D.W.M., L.Z., and T.R.H. synthesized the trilayer garnet. S.X. did electrochemical tests. Y.L. and C.C. did material characterization. All authors contributed in writing the paper.

Notes

The authors declare the following competing financial interest(s): Eric D. Wachsman, Liangbing Hu, and Gregory T. Hitz founded a company to commercialize solid-state batteries. However, all results reported herein were performed at the University of Maryland under federal sponsorship.

ACKNOWLEDGMENTS

The authors would like to thank ARPA-E and NASA for financially supporting this work under the ARPA-E Robust Affordable Next Generation Energy Storage Systems program (Contract No. DE-AR0000384 and DE-AR0000787) and the NASA Advanced Energy Storage System Project within the Game Changing Development Program of the Space Technology Mission Directorate. We would like to acknowledge the characterization facilities at the University of Maryland that enabled much of this work including the FabLab, the AIMlab, the Surface Analysis Center, and the X-ray Crystallography Center.

REFERENCES

(1) Armand, M.; Tarascon, J.-M. *Nature* **2008**, *451*, 652.
(2) Li, Y.; Zhou, W.; Chen, X.; Lu, X.; Cui, Z.; Xin, S.; Xue, L.; Jia, Q.; Goodenough, J. B. *Proc. Natl. Acad. Sci. U. S. A.* **2016**, *113*, 13313.
(3) Huang, C.; Xiao, J.; Shao, Y.; Zheng, J.; Bennett, W. D.; Lu, D.; Saraf, L. V.; Engelhard, M.; Ji, L.; Zhang, J.; Li, X.; Graff, G. L.; Liu, J. *Nat. Commun.* **2014**, *5*, 3015.
(4) Long, J. W.; Dunn, B.; Rolison, D. R.; White, H. S. *Chem. Rev.* **2004**, *104*, 4463.
(5) Guo, Y.; Hu, J.; Wan, L. *Adv. Mater.* **2008**, *20*, 2878.
(6) El-Kady, M. F.; Ihns, M.; Li, M.; Hwang, J. Y.; Mousavi, M. F.; Chaney, L.; Lech, A. T.; Kaner, R. B. *Proc. Natl. Acad. Sci. U. S. A.* **2015**, *112*, 4233.
(7) Xu, W.; Wang, J.; Ding, F.; Chen, X.; Nasybulin, E.; Zhang, Y.; Zhang, J. *Energy Environ. Sci.* **2014**, *7*, 513.
(8) Kim, H.; Jeong, G.; Kim, Y.; Kim, J.; Park, C.; Sohn, H. *Chem. Soc. Rev.* **2013**, *42*, 9011.
(9) Tarascon, J.-M.; Armand, M. *Nature* **2001**, *414*, 359.
(10) Zhang, K.; Lee, G. H.; Park, M.; Li, W.; Kang, Y. M. *Adv. Energy Mater.* **2016**, *6*, 1600811.
(11) Ilott, A. J.; Mohammadi, M.; Chang, H. J.; Grey, C. P.; Jerschow, A. *Proc. Natl. Acad. Sci. U. S. A.* **2016**, *113*, 10779.
(12) Lu, Y.; Tu, Z.; Archer, L. A. *Nat. Mater.* **2014**, *13*, 961.
(13) Tung, S.-O.; Ho, S.; Yang, M.; Zhang, R.; Kotov, N. A. *Nat. Commun.* **2015**, *6*, 6152.
(14) Ryou, M.-H.; Jin Lee, D.; Lee, J.-N.; Min Lee, Y.; Park, J.-K.; Wook Choi, J. *Adv. Energy Mater.* **2012**, *2*, 645.
(15) Wu, H.; Zhuo, D.; Kong, D.; Cui, Y. *Nat. Commun.* **2014**, *5*, 5193.
(16) Luo, W.; Zhou, L.; Fu, K.; Yang, Z.; Wan, J.; Manno, M.; Yao, Y.; Zhu, H.; Yang, B.; Hu, L. *Nano Lett.* **2015**, *15*, 6149.
(17) Li, N.-W.; Yin, Y.-X.; Yang, C.-P.; Guo, Y.-G. *Adv. Mater.* **2016**, *28*, 1853.
(18) Qian, J.; Henderson, W. A.; Xu, W.; Bhattacharya, P.; Engelhard, M.; Borodin, O.; Zhang, J.-G. *Nat. Commun.* **2015**, *6*, 6362.
(19) Tikekar, M. D.; Choudhury, S.; Tu, Z.; Archer, L. A. *Nat. Energy* **2016**, *1*, 16114.
(20) Ji, X.; Liu, D.; Prendiville, D. G.; Zhang, Y.; Liu, X.; Stucky, G. D. *Nano Today* **2012**, *7*, 10.
(21) Yang, C.; Yin, Y.; Zhang, S.; Li, N.; Guo, Y. *Nat. Commun.* **2015**, *6*, 8058.
(22) Lu, L.; Ge, J.; Yang, J.; Chen, S.; Yao, H.; Zhou, F.; Yu, S. *Nano Lett.* **2016**, *16*, 4431.
(23) Zhang, R.; Cheng, X.; Zhao, C.; Peng, H.; Shi, J.; Huang, J.; Wang, J.; Wei, F.; Zhang, Q. *Adv. Mater.* **2016**, *28*, 2155.
(24) Liu, Y.; Lin, D.; Liang, Z.; Zhao, J.; Yan, K.; Cui, Y. *Nat. Commun.* **2016**, *7*, 10992.
(25) Lin, D.; Liu, Y.; Liang, Z.; Lee, H.; Sun, J.; Wang, H.; Yan, K.; Xie, J.; Cui, Y. *Nat. Nanotechnol.* **2016**, *11*, 626.
(26) Zuo, T.; Yin, Y.; Wang, S.; Wang, P.; Yang, X.; Liu, J.; Yang, C.; et al. *Nano Lett.* **2018**, *18*, 297.
(27) Liu, L.; Yin, Y.; Li, J.; Li, N.; Zeng, X.; Ye, H.; Guo, Y.; Wan, L. *Joule* **2017**, *1*, 563.
(28) Luntz, A. C.; Voss, J.; Reuter, K. *J. Phys. Chem. Lett.* **2015**, *6*, 4599.
(29) Li, J.; Ma, C.; Chi, M.; Liang, C.; Dudney, N. J. *Adv. Energy Mater.* **2015**, *5*, 1401408.
(30) Wang, Y.; Richards, W.; Ong, S. P.; Miara, L. J.; Kim, J.; Mo, Y.; Ceder, G. *Nat. Mater.* **2015**, *14*, 1026.
(31) Ihlefeld, J. F.; Clem, P. G.; Doyle, B. L.; Kotula, P. G.; Fenton, K. R.; Apblett, C. A. *Adv. Mater.* **2011**, *23*, 5663.
(32) Yu, R.; Du, Q.; Zou, B.; Wen, Z.; Chen, C. *J. Power Sources* **2016**, *306*, 623.
(33) Feng, J. K.; Yan, B. G.; Liu, J. C.; Lai, M. O.; Li, L. *Mater. Technol.* **2013**, *28*, 276.
(34) Noguchi, Y.; Kobayashi, E.; Plashnitsa, L. S.; Okada, S.; Yamaki, J. *Electrochim. Acta* **2013**, *101*, 59.
(35) Wu, J.; Pang, W. K.; Peterson, V. K.; Wei, L.; Guo, X. *ACS Appl. Mater. Interfaces* **2017**, *9*, 12461.
(36) Wu, J.; Chen, E.; Yu, Y.; Liu, L.; Wu, Y.; Pang, W. K.; Peterson, V. K.; Guo, X. *ACS Appl. Mater. Interfaces* **2017**, *9*, 1542.
(37) Zheng, J.; Tang, M.; Hu, Y. *Angew. Chem., Int. Ed.* **2016**, *55*, 12538.
(38) Thangadurai, V.; Narayanan, S.; Pinzaru, D. *Chem. Soc. Rev.* **2014**, *43*, 4714.
(39) Trevey, J. E.; Jung, Y. S.; Lee, S. *Electrochim. Acta* **2011**, *56*, 4243.
(40) Kato, Y.; Hori, S.; Saito, T.; Suzuki, K.; Hirayama, M.; Mitsui, A.; Yonemura, M.; Iba, H.; Kanno, R. *Nat. Energy* **2016**, *1*, 16030.
(41) Han, X.; Gong, Y.; Fu, K.; He, X.; Hitz, G. T.; Dai, J.; Pearse, A.; Liu, B.; Wang, H.; Rubloff, G.; Mo, Y.; Thangadurai, V.; Wachsman, E. D.; Hu, L. *Nat. Mater.* **2016**, *16*, 572.
(42) Fu, K.; Gong, Y.; Liu, B.; Zhu, Y.; Xu, S.; Yao, Y.; Luo, W.; Wang, C.; Lacey, S. D.; Dai, J.; Chen, Y.; Mo, Y.; Wachsman, E. D.; Hu, L. *Sci. Adv.* **2017**, *3*, e1601659.
(43) Tao, X.; Liu, Y.; Liu, W.; Zhou, G.; Zhao, J.; Lin, D.; Zu, C.; Sheng, O.; Zhang, W.; Lee, H. W.; Cui, Y. *Nano Lett.* **2017**, *17*, 2967.
(44) Park, K.; Yu, B.; Jung, J.; Li, Y.; Zhou, W.; Gao, H.; Son, S.; Goodenough, J. B. *Chem. Mater.* **2016**, *28*, 8051.
(45) van den Broek, J.; Afyon, S.; Rupp, J. L. M. *Adv. Energy Mater.* **2016**, *6*, 1600736.

DOI: 10.1021/acs.nanolett.8b01295
Nano Lett. 2018, 18, 3926−3933

(46) Liu, Y.; Lin, D.; Jin, Y.; Liu, K.; Tao, X.; Zhang, Q.; Zhang, X.; Cui, Y. *Sci. Adv.* **2017**, *3*, eaao0713.
(47) Porz, L.; Swamy, T.; Sheldon, B. W.; Rettenwander, D.; Fromling, T.; Thaman, H. L.; Berendts, S.; Uecker, R.; Carter, W.; Chiang, Y. *Adv. Energy Mater.* **2017**, *7*, 1701003.
(48) Hitz, G. T.; McOwen, D. W.; Zhang, L.; Ma, Z.; Wen, Y.; Gong, Y.; Dai, J.; Hamann, T. R.; Hu, L.; Wachsman, E. D. *Mater. Today* **2018**, DOI: 10.1016/j.mattod.2018.04.004.
(49) Yang, Y.; Zheng, G.; Cui, Y. *Energy Environ. Sci.* **2013**, *6*, 1552.
(50) Fu, K.; Gong, Y.; Hitz, G. T.; McOwen, D. W.; Li, Y.; Xu, S.; Wen, Y.; Zhang, L.; Wang, C.; Pastel, G.; Dai, J.; Liu, B.; Xie, H.; Yao, Y.; Wachsman, E. D.; Hu, L. *Energy Environ. Sci.* **2017**, *10*, 1568.
(51) Wang, C.; Gong, Y.; Liu, B.; Fu, K.; Yao, Y.; Hitz, E.; Li, Y.; Dai, J.; Xu, S.; Luo, W.; Wachsman, E. D.; Hu, L. *Nano Lett.* **2017**, *17*, 565.

DOI: 10.1021/acs.nanolett.8b01295
Nano Lett. 2018, 18, 3926−3933